Glass Molding Tools Fabricated with Selective Laser-induced Etching for Sustainable Treatment of Solid-State Electrolytes

Christian Peters*[1], Benjamin Geppert[1], Enkhtsetseg Dashjav[2], Martin Kratz[1], and Frank Tietz[2]

[1]*Fraunhofer ILT - Institute for Laser Technology, Steinbachstr. 15, 52074 Aachen, Germany*
[2]*Forschungszentrum Jülich GmbH, Wilhelm-Johnen-Str., 52428 Jülich, Germany*
**Corresponding author's e-mail: christian.peters@ilt.fraunhofer.de*

Selective laser-induced etching enables the high-precision fabrication of three-dimensional components from transparent materials. First, ultrashort pulsed, tightly focused laser radiation is used to create a modification within the bulk of the transparent material. By selectively moving the focus, entire contiguous surfaces and volumes can be modified. Subsequently, the modified areas are etched free using an etching liquid. Thus, the desired three-dimensional component is exposed and separated from the surrounding material. Using the SLE process, molding tools made of fused silica are fabricated with functional structures of less than 150 µm in size. By molding the solid-state electrolyte foil of a sodium-based battery cell, the contact areas between the chemical components are increased to enhance the power density. Different structural geometries and dimensions are compared to increase this effect.
DOI: 10.2961/jlmn.2024.01.2014
Keywords: selective laser-induced etching, SLE, molding tools, sodium-based battery

1. Introduction

The so-called Selective Laser-induced Etching (SLE) is a fabrication method to produce high-precision, three-dimensional components from transparent materials. The SLE process is a three-step process. Basis is a CAD drawing of a three-dimensional component or geometry that is to be produced from an existing transparent material. Based on this drawing, scanning vectors are first calculated. For this purpose, the CAD model is sliced in z direction into several layers. Scanning vectors are then generated along the surface of the three-dimensional object and the defined slicing distance z. Based on these calculated scanning vectors the material is structured in a subsequent laser processing step. For this purpose, ultrashort pulsed (USP) laser radiation is tightly focused into a dielectric material. The high intensities achieved inside this focus volume (>10^{12} W/cm^2) lead to an energy deposition of the photons inside the dielectric due to non-linear absorption effects (multi-photon absorption, tunnel ionization, etc.) [1]. This leads to the formation of local in-volume modifications. By selectively moving the laser focus along the previously calculated scanning vectors, large areas inside the transparent material are modified. Depending on the selected laser parameters, the resulting modifications differ in their physical and chemical properties [2]. The induced modifications also have a higher etchability to acids and alkalis. The third process step involves a wet chemical etching process in which the processed sample is exposed to an etchant in an ultrasonic bath. During the etching process lasting several hours, the modified areas are completely removed and the surrounding structures or the three-dimensional components are exposed. The etching liquid is heated to increase the reactivity. One quantifiable variable in this process is the selectivity S:

$$S = \frac{\rho_{(mod.)}}{\rho_{(unmod.)}} + 1 \quad (1)$$

The selectivity is the ratio of the etch rate of the modified material $\rho_{(\mathrm{mod.})}$ [µm/h] to the etch rate of the unmodified material $\rho_{(\mathrm{unmod.})}$ [µm/h] [3, 4]. The SLE process has now been developed for a variety of different materials such as fused silica [3, 5–7], sapphire [8–10] and borosilicate glass [11]. For fused silica in particular, the process has also been researched for a wide range of etching liquids and process parameters. Selectivities of more than 1400:1 have been achieved for the SLE process with potassium hydroxide (KOH), which enables the fabrication of three-dimensional structures with micrometer precision [3]. The applications of the process are numerous and range from the medical [7, 12–14] and sensor [15, 16] industries to the production of optics [17, 18] and hardware for quantum technology [19, 20]. A new field of application is the production of molding tools made of glass for battery technology. Due to the constant expansion of volatile energy sources, such as solar and wind, there is an increasing need for reliable energy storage systems that can compensate the differences in energy balances that occur on a daily or annual basis [21–23]. One possibility is the short-term storage of electrical energy using (solid-state) batteries [24]. In particular, lithium and sodium solid-state batteries are seen as the energy storage devices of the future due to their high energy density, long life and safe operation [25]. For the approach of solid state batteries the ion conducting electrolyte is provided as a solid state separator material. In the present case it is an Na-ion conducting Na-Si-Zr-P-O based tape-casted oxide material (NZSP). Due to the wide availability and lower costs of raw materials as well as lower toxicity, sodium-based batteries represent a more sustainable and resource-saving alternative compared to Li

batteries [26, 27]. However, one challenge for the development of practical application is the poor wettability between the solid-state electrolyte and the electrode materials. Here, laser processes can be used to microstructure the separator material to improve the contacting to the electrodes (in the present work it is the cathode side) and therefore improve the interface stability during the co-firing step in the process chain. In addition, the surface enlargement leads to a minimization of the contact resistances arising at the interfaces, which are largely responsible for a power loss of the battery cells at room temperature [28]. This can also lead to an improvement of the power density without decreasing the energy density of the battery cell. There are various approaches to increase the surface area of the active materials. For example, with the help of an USP laser process, the active material can be directly ablated. Thus, various structures for surface enlargement can be created. This work focuses on an alternative approach, which inserts such surface-enhancing structures using SLE-fabricated glass stamps. Due to its material-specific properties, in particular the high softening temperature of 1585 °C [29–32] and a hardness of 5.5 - 6.5 on the Mohs hardness scale [30], fused silica is a promising base material for the fabrication of molding tools. The stamps are fabricated with very small periodic structures in the order of ~150 µm, which are pressed into a solid-state electrolyte film during a molding process. This paper describes the manufacturing process of such molding tools with different structural geometries and sizes using the SLE process.

In the following chapter 1.1 the basic design of the glass mold is presented and the different structures that are molded in the solid electrolyte are explained in more detail. The following chapter 1.2 deals with the experimental setup as well as the limitations and challenges of the SLE process for the fabrication of glass molds. Based on this, the shape fidelity and surface properties of the SLE fabricated stamp structures are examined in more detail (chapter 2.1, 2.2 & 2.3). An electrochemical measurement of the functionalized solid-state electrolyte foils and a critical evaluation of the results will be carried out in chapter 2.4 to finally assess the suitability of the SLE process as a manufacturing process for molding tools in the course of functionalizing solid-state batteries to increase the power density.

1.1 Molding tool design

The molding tool is used to functionalize a circular disc of the solid-state electrolyte material NZSP (diameter 10 mm) with a thickness of approximately 200 µm. During the molding process, the solid-state electrolyte must not be damaged or penetrated, as this would lead directly to short circuits inside the battery. At the same time, the aim is to achieve the greatest possible surface enlargement effect. Therefore, several geometries and structure densities are evaluated. Simultaneously, a simple specimen handling must be ensured, which guarantees the damage-free and repetitive molding process with the manufactured stamps. With these criteria in mind, the following stamp design is developed.

The basic design of the molding tool is shown in Figure 1.

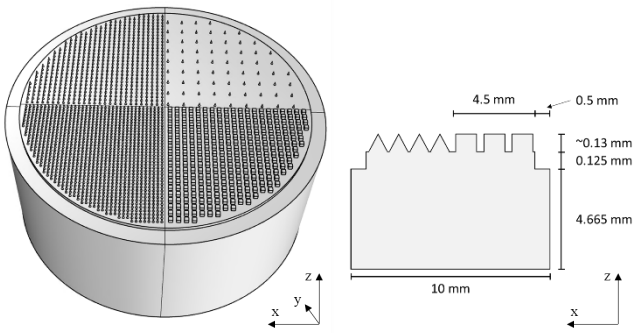

Fig. 1 CAD model of the molding tool (left). Dimensions of four different structures (right).

The stamp is made of fused silica (Siegert Wafer GmbH) and has a diameter of 10 mm and a total height of ~ 4.9 mm. Four different structures are applied around the center of the stamp, each in a quarter circle with an edge length of 4.5 mm (see Figure 1, right). The structures differ in geometric shape (cone or square), dimension (diameter or edge length) and distance from each other. The height of each structure is 110 µm. A 500 µm wide margin with a depth of 125 µm below the stamp surface is present between the structures and the stamp edge. During the molding process, this offset margin simplifies the handling of the sample, especially the removal of the molded solid electrolyte foils.

The fabrication of the glass stamps poses a challenge in terms of the low defect tolerance that is aimed for. Missing or damaged structures as well as residues remaining on the stamps lead to damage to the electrolyte foil or glass residues in the molded structures, resulting in a permanent reduction of the battery cell functionality. The desired dimensions of the structures are summarized in Table 1.

Table 1 Targeted structure sizes.

Geometry	Height	Diameter / Edge length	Distance
Cone I	110 µm	60 µm	130 µm
Cone II	110 µm	60 µm	180 µm
Cone III	110 µm	60 µm	540 µm
Cube	110 µm	120 µm	240 µm

1.2 Experimental Setup and fabrication process

A schematic illustration of the experimental setup is shown in Figure 2.

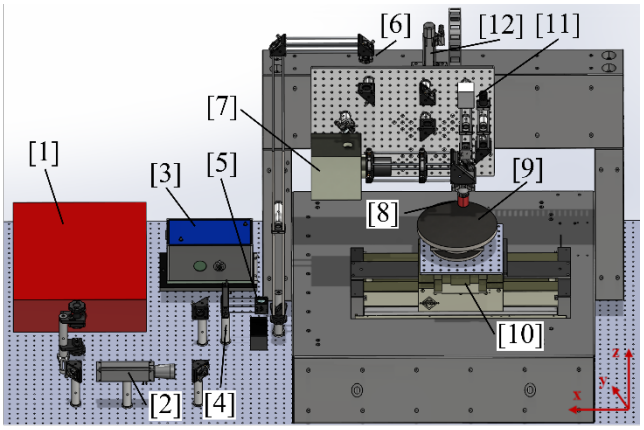

[1] USP laser source [5] Pol. beamsplitter [9] Chuck
[2] Telescope [6] λ/4 plate [10] x-y-Axis
[3] Autocorrelator [7] Scanner [11] Camera
[4] λ/2 plate [8] Objective [12] z-Axis

Fig. 2 Schematic illustration of the experimental setup. The glass probe is placed on the chuck with its surface perpendicular to the beam propagation.

The USP laser source used for the generation of sustainable modifications is the Amplitude *Satsuma HP* system. This laser emits light of wavelength $\lambda = 1030$ nm with an average power of up to $\overline{P} = 10$ W at repetition rates in the range of $f_{Rep} = 1$ Hz to 40 MHz and pulse durations in the region of $\tau = 380$ fs to 10 ps. The raw beam diameter is expanded to $d_{raw} = 6$ mm with the aid of a telescope (*OPTOGAMA, MEX18*). This beam diameter is necessary to fully illuminate the input aperture of the focusing optic. This is then followed by a beam splitter and quarter-wave plate to generate circular polarized light. The polarization of the light in dependence of the structuring direction has a massive influence on the formation of periodic nanocracks which strongly affect the etching behavior of the modifications [2]. Thus, circular polarized light is utilized for uniformity of the modification direction. The polarization plate is followed by a microscanner system consisting of a galvanometer scanner (SCANLAB *intelliSCAN$_{se}$ 14*) and focusing optic (Mitutoyo *M Plan Apo NIR 20x/0.4*). The optical components including the scanner system are mounted on a mechanically supported linear stage (Aerotech *ATS50030*). Below the focusing optics, a vacuum chuck (Light-Fab) is mounted on an air-bearing axis system (Aerotech *ABL20030* and *ABL10100-LN*). With the aid of an alignment stage the sample material is aligned to the focusing optics with micrometer precision. During the laser material treatment, the focus is moved along the calculated scanning vectors inside the sample with the scanner system. The two axis system keeps the position of the sample constant relative to the focusing optics at this time. The maximum scan field has the dimension of 500 x 500 µm^2. The size of this scan field is limited by the focusing optics. In order to be able to structure larger areas than the scan field, the stitching of several scan fields is necessary. Starting on the bottom side of the sample, contiguous modification areas are thus introduced into the transparent material level by level. An increasing sample depth yields spherical aberrations which lead to an increase of the focal volume and to a decrease of the maximum intensity [4]. In order to reach the threshold intensity for absorption of the laser radiation in the dielectric, the average power of the laser radiation (pulse energy) is increased. With decreasing structuring depth, the pulse energy is linearly reduced from 987 nJ (sample bottom side) to 283 nJ (sample surface). This corresponds to a power correction of 141 nJ/mm.

The process parameters used for the fabrication of the glass stamps are summarized in Table 2 below.

Table 2 Process parameters used for the fabrication of glass stamps.

Parameter	Value
Wavelength	1030 nm
Repetition rate	760 kHz
Pulse duration	1 ps
Focus diameter	3,6 µm
Scan speed	200 mm/s
Pulse energy	283 – 987 nJ
Depth correction pulse energy	141 nJ/mm
Polarization	circular
Etching liquid	Potassium hydroxide (KOH)
KOH concentration	8 mol/l
Etching temperature	85 °C
Etch duration	24-28 h
Ultrasonic frequency	35 kHz
Material	Fused silica
Slicing distance z	5 µm
Hatch distance	5, 20, 100, 150 µm

The SLE process is subject to various limitations due to the complex process chain (CAD-CAM, laser modification, wet chemical etching) and physical and chemical boundary conditions. These must be considered during the fabrication of three-dimensional components and can only be partially corrected by adjusting the process parameters. The most important effects are:

- **Laser induced stress:** As a result of the energy deposition within the transparent material, modifications with different density and refractive index compared to the surrounding material are formed. The formation of these modifications leads to short-term and sustained mechanical stresses inside the material, which can be discharged in micro- and nano-cracks. As the number of modifications per volume increases, the induced stresses and the probability of cracks and damage increase as well. It is therefore not possible to fully structure large contiguous areas or volumes so that they are removed during the etching process.
- **Decreasing precision with sample thickness:** The etching process is highly complex and depends on many external factors (e.g. choice and concentration

of etching liquid, ultrasonic frequency, temperature). Starting at the component surface, the acid or alkali etches through the modification lines into the interior of the material. With increasing time and structuring depth, the etching rate decreases [33]. Modified and unmodified structures, which are close to the component surface are exposed to the etchant for much longer than modifications further below the component surface. This leads to a loss of dimensional accuracy, especially for structures close to the surface.

In order to minimize stress, the risk of crack centers and damages during the stamp manufacturing process a concept of different scanning strategies with various line spacings (hatch distance, see Table 2) is used to keep the amount of modification lines per volume as low as possible. The volume around the structures is filled with a grid-like network of modification lines oriented perpendicular to each other. During the etching process, this scanning strategy creates small glass cubes that are separated from the component. This means that the entire volume that has to be removed does not have to be modified completely. This shortens the process time and reduces stresses within the sample material. The peaks of the structures are located 100 µm below the sample surface (with respect to the beam propagation) in order to have a safety distance to the probe surface to ensure that all critical modification lines (stamp structures) lay inside the sample material. With this proceed misalignments and quality irregularities of the raw material can be compensated. The distance of 100 µm is not increased to minimize spherical aberrations and increase shape fidelity after the etching process. In greater depth only the surface of the cylindrical shape of the stamp is structured into the glass raw material. Since the dimensional accuracy of the cylindrical surface of the stamp is of no significant importance for the final application, the use of an aberration-compensating process, for example by using a Spatial Light Modulator (SLM), is not used at this point [4].

The fabricated glass stamps are analyzed and measured using a digital microscope (Keyence *VHX 6000*), a white light interferometer (Zygo *Nexview™ NX2*), a laser scanning microscope (Keyence *LSM VK-9700*) and a scanning electron microscope (ThermoFischer *Apero 2*). In addition, with the aid of a micro-computer tomograph (micro-CT), images of the cross-sectional profile of the stamp are created using high-energy X-rays. By combining a large number of individual images, it is thus possible to create three-dimensional images of the molding tool.

During process development and proof-of-principle for the functionalization of solid-state batteries using SLE fabricated glass stamps, the molding process is performed by hand. This is to avoid damage to the sample material, especially the solid-state electrolyte foil, by the sensitive feedback. For the subsequent standardization of the molding process, a hydraulic press with individually adjustable contact pressure and duration is used.

2. Results

2.1 Analysis of the form fidelity of the fabricated glass stamps

The total time required to manufacture a stamp is around 30 hours. Laser structuring lasts about 5 hours of this time and the etching time is approximately 25 hours. Figure 3 shows a fabricated glass stamp after the SLE process. In more detail, Figure 4 displays an image of a stamp surface taken with the Keyence *VHX 6000* microscope. None of the total of approximately 4300 manufactured structures shows any damage or visible cracks.

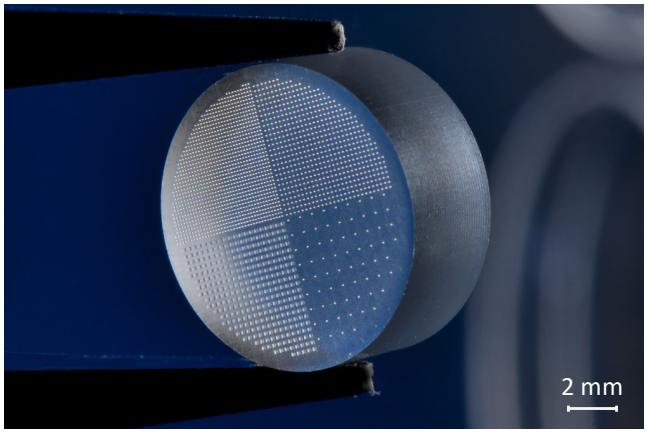

Fig. 3 Picture of a glass stamp fabricated using SLE.

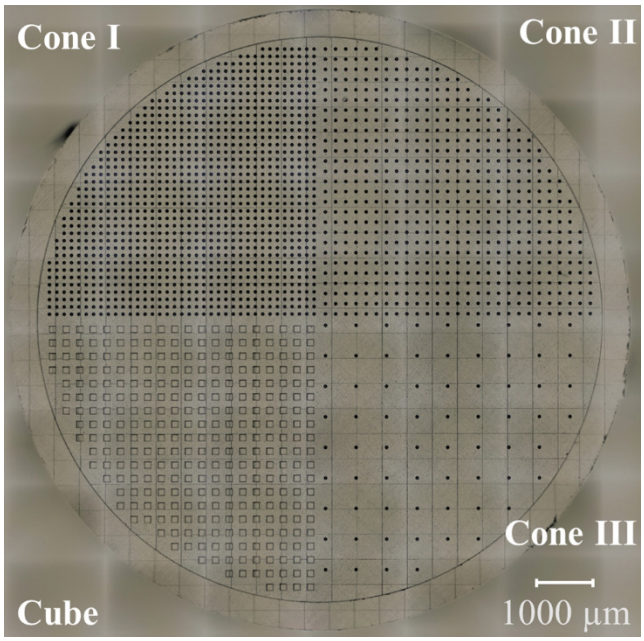

Fig. 4 Panoramic image of the surface of a glass stamp. Due to the limited measuring range of the Keyence *VHX 6000*, several images are combined to form a panoramic image.

Due to the optics and beam shape of the utilized laser, the focus position of the laser is not exactly at one z height over the entire area of a scan field. This results in the average power of the laser beam decreasing in a plane towards the edges of the scan field. As a result of the stitching of several scan fields, a gradual transition (also called scan field tilt) of up to 4 µm can occur at the edge areas of the scan fields. This can be seen in the panoramic image as a grid-like structure on the stamp surface. This is irrelevant for the subsequent application since the stamp structures are not completely pressed into the electrolyte foil during the moding process. Therefore, it is decided not to optimize the scan field tilting.

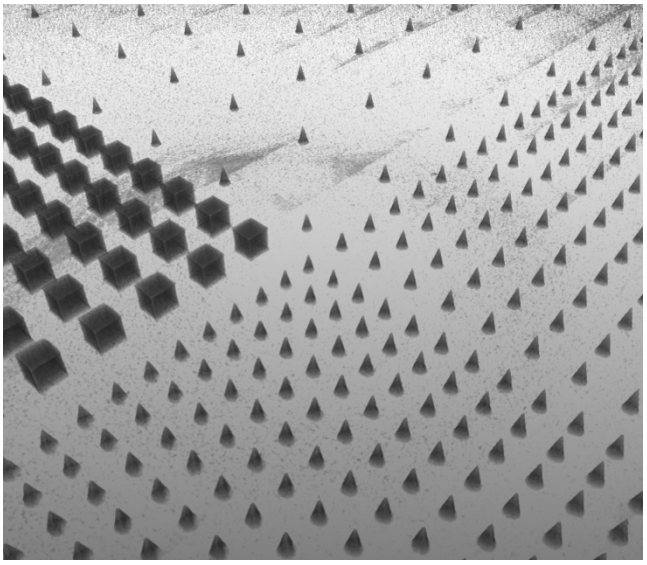

Fig. 5 Imaging of the stamp surface using a micro-CT.

In order to analyze the condition of the structures a micro-CT image of the stamp surface is recorded. No damages and/or cracks are visible on the surface of the structure or within the individual structures. Furthermore, no glass residues are visible on the stamp surface.

Table 3 below summarizes the real structure sizes of the glass stamp after the SLE process. Several structures are measured and the arithmetic mean was calculated. The measuring equipment used is the digital microscope (Keyence *VHX 6000*), white light interferometer (Zygo *Nexview™ NX2*) and laser scanning microscope (Keyence *LSM VK-9700*).

Table 3 Structure size after SLE process.

Geometry	Height	Diameter / Edge length	Distance
Cone I	113 µm	58 µm	130 µm
Cone II	110 µm	60 µm	180 µm
Cone III	114 µm	60 µm	540 µm
Cube	117 µm	125 µm	240 µm

Due to the high feed accuracy of the air-guided axis system (~ 0.3 µm), there are no measurable deviations between the targeted and measured distances of the structures. The height of the structures differs on average by a maximum of 7 µm from the target size. These values correspond to the measured deviations for the diameter and edge length, which amount to a maximum of 5 µm. Due to the above-mentioned limitations in the SLE process, in particular the 2.5 dimensional approximation of the three-dimensional component and the complex etching process, the fabrication process is limited to the determined form fidelity of the structures. The reproducibility and low defect tolerance of the structures are particularly important for use as a molding tool. This has been proven to be achieved (see Figure 3-5).

2.2 Analysis of the surface texture of the fabricated glass stamps

For the suitability as a molding tool, especially for solids, the surface quality of the molding structures is of essential importance. Preliminary tests comparing molding tools made of glass and metal (stainless steel) showed that thermal processes during laser material processing of stainless steel lead to the formation of melts and associated particle residues on the stamp surface (see Figure 6).

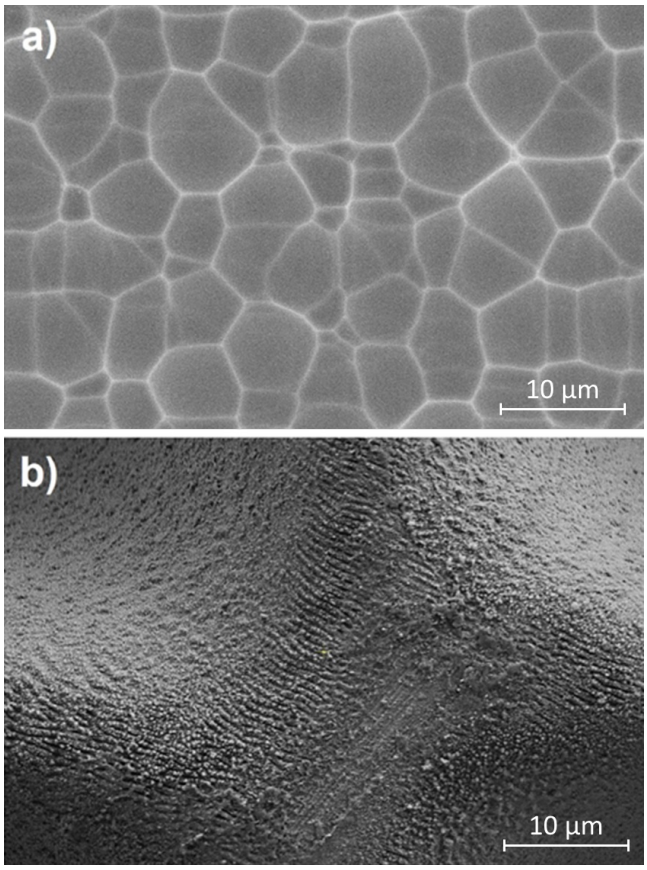

Fig. 6 Comparison of the surface nature of different materials used for molding tools. a) SLE produced fused silica surface, b) direct laser structured stainless steel.

SLE processed fused silica for use as molding tool material shows a very smooth surface nature compared to steel based materials processed by direct laser structuring. No particle residues or surface structures with sharp edges are visible. The surface roughness (RMS) of different manufactured stamps was measured with the Zygo Nexview™ NX2 light interferometer and is ~230-530 nm, which matches well with values from the literature [6]. Therefore, we suspect that glass based SLE processed materials facilitate sample handling during the molding process and probably lead to minor contamination and damaging of the electrolyte material.

Figure 7 shows detailed SEM images of the structures on the stamp surface.

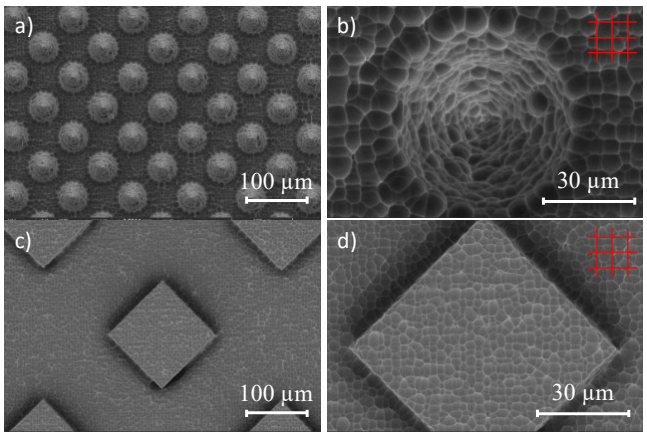

Fig. 7 SEM images of different structures with alignment of the grid-like mesh of scan vectors (in red). a) Panorama image of Cone I, b) Cone I, c) Panorama image of Cube, d) Cube.

As shown in the SEM images, the surface of the stamp exhibits the typical SLE surface texture (see also Figure 6 a)). The remarkable periodicity of the individual scales composing the surface is probably a consequence of the chosen structuring strategy. The surface is filled with a grid-like mesh of scanning vectors oriented perpendicular to each other (see Figure 7 b) & d)). The line spacing is chosen small enough (5 µm) that it is completely etched during the etching process. This separates the glass volume above the stamp surface from the rest of the stamp but leads to small horizontal etching channels which form the grid-like surface structure. Due to the irregular etching process, the etch rate is slightly different at different points on the stamp, so that the shape and dimensions of the scales vary. It is interesting to note that the scaly surface structure is also continued on the structures, in particular on the cone surfaces. Contrary to the stamp surface, however, the surface texture there is oriented into the stamp surface structure. Our assumption is that these multiple modifications, induced during the laser processing, experience increased etchability and form the inwardly oriented scales. The surface of the stamp and structure are completely free of particles and damage, and also have no structures potentially damaging to the solid-state electrolyte.

2.3 Molding process

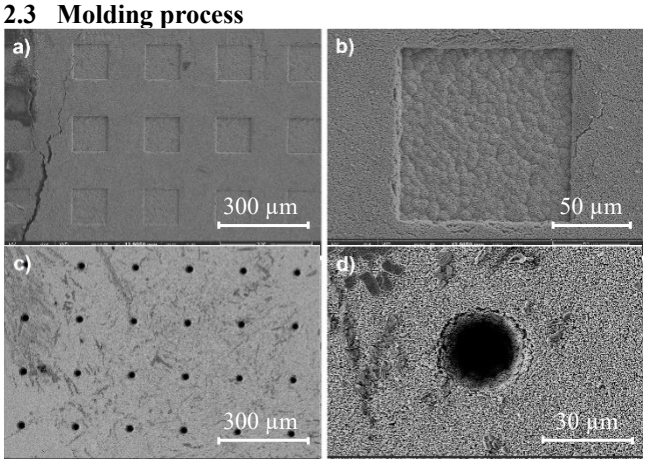

Fig. 8 Electron micrographs of the imprinted stamping structures into Na-Si-Zr-P-O based green tape. a) and b) imprint of cube-like structures, c) and d) imprint of cone-like structures (Cone II).

Several samples of the solid state electrolyte (NZSP) are processed with the stamps described in chapter 1.1. Figure 8 shows SEM images of the molded structures in the solid state electrolyte. Using an LSM microscope, a profile analysis of the molded structures shown in Figure 8 is performed. The results are plotted in Figure 9.

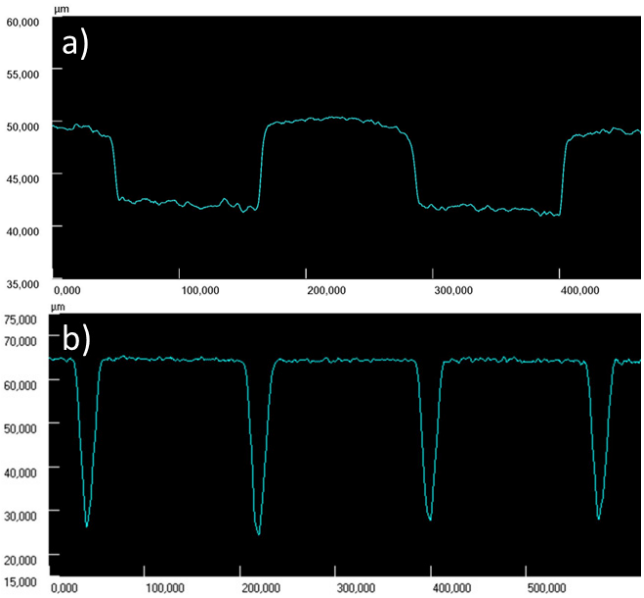

Fig. 9 Laser microscopic profiles of the imprinted stamping structures in Na-Si-Zr-P-O green tape. a) Imprint of cube-like structures, b) imprint of cone-like structures (Cone II).

As depicted in Figure 8, a molding process is successfully carried out. During the molding process, both the stamp and the stamp structures remain undamaged. For the square-shaped structure, it can be clearly seen that the SLE-induced surface texture is molded into the solid-state electrolyte during the molding process. The depth of the molded structures is about 7 µm for the cuboid structures and about 36 µm for the cone structures. As an example, Figures 8 and 9 show the results of the molding processes with the Cone II cone-shaped structures. The results of the Cone I and Cone III structures match those of the Cone II structures within the measurement accuracies of the SEM used.

2.4 Battery fabrication & electrochemical measurements

Based on the results described in chapter 2.1 - 2.3, a glass stamp with only the Cone II structure is manufactured using SLE and then used for the fabrication of a functionalized battery cell. On the one hand, this structure (Cone II) is characterized by a higher molding depth of the structures compared to the square-shaped structure (see Figure 9) and, on the other hand, the structure spacing of 180 µm is ideally suited for the functionalization of the solid-state electrolyte film. During the molding process, the stamps with a structure spacing of 120 µm require a higher contact pressure than the stamps with a structure spacing of 180 µm, which increases the risk of damage to the solid-state electrolyte film. A distance of 540 µm has only a low structure density, so that the surface enlargement due to functionalization will be very small and the effect of increasing the power density will be low. As a compromise between sample handling during

the molding process and the greatest effect on the increase in power density, a stamp with the Cone II structure is selected for the fabrication of a functionalized battery cell.

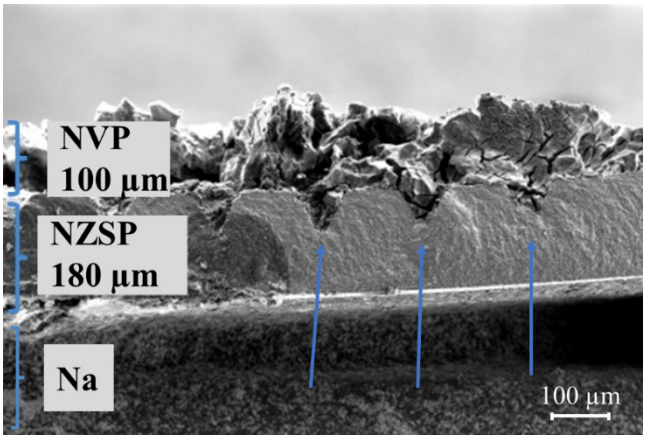

Fig. 10 SEM image of a functionalized battery cell. The solid electrolyte foil is imprinted by a glass stamp with Cone II structure (green arrows).

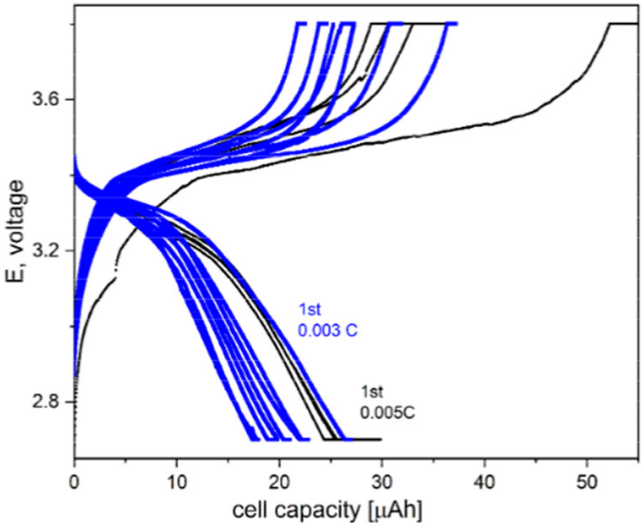

Fig. 11 Voltage over cell capacity for different C-rates. Blue: 0.003 C and Black: 0.005 C.

Figure 10 shows a cross-sectional SEM image of an already sintered battery cell. In the middle layer (solid electrolyte foil) the molded cone structures are clearly visible. During the sintering process, these are completely infiltrated by the cathode material. A sodium layer is used as the anode material. Several charge and discharge cycles are measured to verify the functionality of the battery cell. Figure 11 shows the measured voltage versus the calculated cell capacity for different C rates.

The maximum cell capacity measured for both C rates is around 25 µAh.

3. Conclusion

This work demonstrates the fabrication of glass molds by SLE for the functionalization of sodium-based solid-state batteries. In total, four different structures are evaluated with respect to the feasibility of fabrication by the SLE process and their suitability for the molding process. For this purpose, the surface properties and the shape fidelity of the fabricated structures are analyzed by means of optical microscopy, a scanning electron microscope and a micro-CT. It is shown that the SLE process is particularly suitable for the fabrication of impression tools due to its particle-free and smooth surface, especially compared to metals. The structures produced exhibit a maximum deviation of 7 µm from the target geometry on average. Subsequently, an impression test is carried out in which the glass stamp is pressed into an NSZP solid electrolyte foil. As a result of the molding process, the structure "Cone II" with an impression depth of ~ 36 µm is selected as the most promising approach for the fabrication of a functionalized solid state battery cell. Based on the results obtained, a functionalized, functional battery cell is fabricated and electrochemical measured during several load and unload cycles. The maximum measured cell capacity was ~ 25 µAh.

Molding tools made of glass are not only suited for industrial use due to their material-specific properties (high softening temperature and degree of hardness). In combination with the SLE process, three-dimensional structures can be produced with micrometer precision, individually optimized to the application. One advantage over metal molds produced with laser-based manufacturing processes is the surface quality of components fabricated using SLE. The surface is free of particles and has a low surface roughness of less than 1 µm (RMS), which can be further reduced with the aid of laser polishing processes. However, the use of glass molding tools is not limited to battery technology. All application areas that require a temperature and pressure resistant molding tool as well as a flexible design of the molded structures can benefit from these tools fabricated with SLE. After the proof of principle, further tests with different structures, structure densities and a standardized molding process are pending. By using the SLE process, additional features such as cooling channels can be added to the impression tool in the future. The fabrication of the stamps from another material, such as sapphire, is also an option to improve the quality of the molding tool. Compared to glass, sapphire has a significantly higher degree of hardness (9 on Mohs scale) and seven times higher thermal conductivity (12,58 [W/Km])) which is a great advantage for implementation in an industrial process [30, 34, 35]. In addition, the selectivity of nearly 10,000 during the SLE Process enables the production of structures that are almost perfectly accurate in terms of shape fidelity [36].

The SLE process is characterized by high precision and flexibility in the choice of structure geometries. But the manufacturing process of a stamp is comparatively com-plex and therefore expensive due to the long structuring time of 5 hours. Due to the symmetrical design and the high periodicity of the structures, the laser structuring process could be scaled using parallelized laser processes, such as multi-beam processing. Here, the beam is split into a matrix of partial beams using an SLM. With the help of this matrix of partial beams, many modification lines can be generated simultaneously. This would lead to a significant reduction in the structuring time, which would also enable the production of larger stamps with a greater number of structures. Limits of this process is the maximum number of beams inside a single scan field which depends on the distance between to different structures and the scan field dimension. Furthermore, a laser source with a higher average power than for single beam processing is required.

References

[1] C. Kalupka: "Energiedeposition von ultrakurz gepulster Laserstrahlung in Gläsern; 1. Auflage", (Apprimus Verlag, Aachen, 2019) p.6.
[2] R. Taylor, C. Hnatovsky, and E. Simova: Laser Photonics Rev., 2, (2008) 26.
[3] J. Gottmann, M. Hermans, N. Repiev, and J. Ortmann: Micromachines, 8, (2017) 110.
[4] M. Kratz, L. Rückle, C. Kalupka, M. Reininghaus, and C. L. Haefner: Opt. Express, 31, (2023) 26104.
[5] M. Hermans, J. Gottmann, and F. Riedel: J. Laser Micro Nanoeng., 9, (2014) 126.
[6] A. Butkutė, T. Baravykas, J. Stančikas, T. Tičkūnas, R. Vargalis, D. Paipulas, V. Sirutkaitis, and L. Jonušauskas: Opt. Express, 29, (2021) 23487.
[7] S. Kim, J. Kim, Y.-H. Joung, S. Ahn, J. Choi, and C. Koo: Micro and Nano Syst. Lett., 7, (2019) 15.
[8] M. Hörstmann-Jungemann, J. Gottman, and M. Keggenhoff: J. Laser Micro Nanoeng., 5, (2010) 145.
[9] M. Hörstmann-Jungemann, J. Gottmann, and D. Wortmann: J. Laser Micro Nanoeng., 4, (2009) 135.
[10] L. Capuano: "Laser micro/nanoprocessing and subsequent chemical etching of sapphire for surface and bulk functionalization", (Enschede, 2020) p.84.
[11] D. Bischof, M. Kahl, and M. Michler: Opt. Mater. Express, 11, (2021) 1185.
[12] R. Osellame, V. Maselli, R. Vazquez Martinez, R. Ramponi, and G. Cerullo: Appl. Phys. Lett., 90, (2007) 231118.
[13] R. Osellame, H. Hoekstra, G. Cerullo, and M. Pollnau: Laser Photonics Rev., 5, (2011) 442.
[14] K. Sugioka and Y. Cheng: Lab Chip, 12, (2012) 3576.
[15] F. He, Y. Liao, J. Lin, J. Song, L. Qiao, Y. Cheng, and K. Sugioka: Sensors, 14, (2014) 19402.
[16] J. Song, J. Lin, J. Tang, Y. Liao, F. He, Z. Wang, L. Qiao, K. Sugioka, and Y. Cheng: Opt. Express, 22, (2014) 14792.
[17] J.-L. Skora, O. Gaiffe, S. Bargiel, J.-M. Cote, L. Tavernier, M. de Labachelerie, and N. Passilly: Opt. Express, 30, (2022) 3749.
[18] B. McMillen, C. Athanasiou, and Y. Bellouard: Opt. Express, 24, (2016) 27239.
[19] S. Simeth, A. Müller, J. Müller, B. Lekitsch, M. Reininghaus, and F. Schmidt-Kaler: Proc. SPIE, Vol. 12409, (2023) 1240902.
[20] G. Corrielli, A. Crespi, and R. Osellame: Nanophotonics, 10, (2021) 3789.
[21] Bent Sørensen: "Renewable Energy Conversion, Transmission and Storage", (Elsevier Inc., Gilleleje, 2007) p.1.
[22] S. Ould Amrouche, D. Rekioua, T. Rekioua, and S. Bacha: Int. J. Hydrog. Energy, 41, (2016) 20914.
[23] H. Zhao, Q. Wu, S. Hu, H. Xu, and C. Nygaard Rasmussen: Appl. Energy, 137, (2015) 545.
[24] B. L. Ellis and L. F. Nazar: Curr. Opin. Solid State Mater. Sci., 16, (2012) 168.
[25] S. Wang, H. Xu, W. Li, A. Dolocan, and A. Manthiram: J. Am. Chem. Soc., 140, (2018) 250.
[26] H. Pan, Y. S. Hu, and L. Chen: Energy Environ. Sci., 6, (2013) 2338.
[27] D. Kundu, E. Talaie, V. Duffort, and L. F. Nazar: Angew. Chem., 54, (2015) 3431.
[28] M. Finsterbusch, T. Danner, C.-L. Tsai, S. Uhlenbruck, A. Latz, and O. Guillon: ACS Appl. Mater. Interfaces, 10, (2018) 22329.
[29] R. N. Widmer, D. Bischof, J. Jurczyk, M. Michler, J. Schwiedrzik, and J. Michler: Mater. Des., 204, (2021) 109670.
[30] Heraeus Conamic: "Properties of Fused Silica", https://www.heraeus.com/en/hca/fused_silica_quartz_knowledge_base_1/properties_1/properties_hca.html#tabs-608478-1, (19.07.2023).
[31] Corning Incorporated: "HPFS® Fused Silica Standard Grade, Corning code 7980", https://www.corning.com/media/worldwide/csm/documents/HPFS_Product_Brochure_All_Grades_2015_07_21.pdf, (19.07.23).
[32] J. David Musgraves, J. Hu, and L. Calvez: "Springer Handbook of Glass", (Springer, Cham, 2019) p.51.
[33] A. Butkutė, G. Merkininkaitė, T. Jurkšas, J. Stančikas, T. Baravykas, R. Vargalis, T. Tičkūnas, J. Bachmann, S. Šakirzanovas, V. Sirutkaitis, and L. Jonušauskas: Materials (Basel, Switzerland), 15, (2022) 2817.
[34] V. Pishchik, L. A. Lytvynov, and E. R. Dobrovinskaya: "Sapphire", (Springer US, Boston, MA, 2009) p.55.
[35] Klein & Becker: "Eigenschaften von Saphir", http://www.klein-becker.com/files/downloads/Eigenschaften%20Saphir.pdf, (19.07.2023).
[36] S. Juodkazis, K. Nishimura, H. Misawa, T. Ebisui, R. Waki, S. Matsuo, and T. Okada: Adv. Mater., 18, (2006) 1361.

(Received: July 28, 2023, Accepted: February 12, 2024)